Palladium Monophosphine Intermediates in Catalytic Cross-Coupling Reactions: A DFT Study

Lukas J. Goossen,*,† Debasis Koley, Holger L. Hermann, and Walter Thiel*

Max-Planck-Institut für Kohlenforschung, D-45470 Mülheim an der Ruhr, Germany

Received August 8, 2005

The mechanism of the cross-coupling of phenylboronic acid with acetic anhydride, a viable model of the widely used Suzuki reaction, has been studied by DFT calculations at the BP86/6-31G* level of theory. Multiple interconnected reaction pathways are considered that start from the neutral $Pd(PMe_3)_2$ molecule, the two-coordinate anionic $[Pd(PMe_3)OAc]^-$ complex, and the three-coordinate anionic $[Pd(PMe_3)_2OAc]^-$ complex. The calculated catalytic cycles seem mechanistically and energetically plausible. According to the calculations, oxidative addition of acetic anhydride to either of the two anionic species leads to the formation of anionic palladium(II) monophosphine complexes with two acetate ligands located either cis or trans to each other. As a consequence, there are two competing anionic pathways for the transmetalation reaction with phenylboronic acid which involve only monosphosphine complexes. Both pathways are energetically feasible, with a slight preference for the cis variant. Reductive elimination of the product acetone in the presence of a second phosphine molecule leads to the regeneration of the anionic bisphosphine complex $[Pd(PMe_3)_2OAc]^-$ while the monophosphine complex $[Pd(PMe_3)OAc]^-$ is formed in the absence of excess phosphine. Our calculations suggest that in Suzuki-type coupling reactions several catalytic pathways involving neutral and anionic palladium species may generally contribute to the catalytic turnover. In the present model system, the anionic pathways are most favorable.

1. Introduction

Palladium-catalyzed cross-couplings of boronic acids are powerful transformations, widely applied in organic synthesis.[1] A particularly prominent example is the Suzuki coupling of aryl halides with arylboronic acids, arguably the most general method for the construction of a biaryl moiety (Scheme 1; R, R′ = aryl), and there is a wealth of mechanistically related reactions, including the synthesis of dienes,[2] arylacetic acids,[3] and aryl ketones (Scheme 1).[4,5]

The main components of the catalytic cycles for all these couplings are believed to be an oxidative addition of the carbon electrophile to a coordinatively unsaturated palladium(0) species, followed by a transmetalation step in which the carbon electrophile is transferred from boron to palladium, and finally a reductive elimination to release the product.[1] To rationally design and optimize such cross-coupling reactions, a much more thorough understanding of this mechanism is indispensable. However, in-depth mechanistic studies as well as theoretical calculations on the Suzuki biaryl synthesis are hampered by the extreme complexity of the experimentally employed reaction systems, which in addition to the palladium phosphine catalysts and the substrates (arylboronic acids and aryl halides) also contain bases, coordinating solvents, and further additives such as halide salts.[1] Thus, an incredible variety of palladium species can potentially be formed, which must all be considered as possible intermediates in the catalytic process.

Scheme 1. Suzuki-Type Cross-Coupling Reactions of Boronic Acids

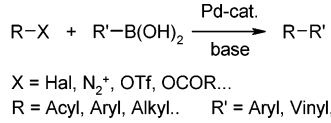

Scheme 2. Cross-Coupling of Acetic Anhydride with Phenylboronic Acid

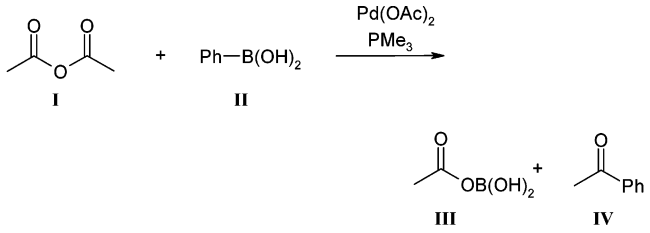

We have previously introduced the mechanistically closely related cross-coupling of acetic anhydride with phenylboronic acid (Scheme 2) as the most basic and still realistic model for a catalytic reaction of this type.[6] The similarity between the oxidative addition steps of aryl halides and carboxylic anhydrides is well documented,[7] and the synthesis of aryl ketones

† Current address: Fachbereich Chemie-Organische Chemie, Technische Universität Kaiserslautern, Erwin-Schrödinger-Strasse Geb. 54, D-67663 Kaiserslautern, Germany. E-mail: goossen@chemie.uni-kl.de.

(1) (a) Miyaura, N.; Suzuki, A. *Chem. Rev.* **1995**, *95*, 2457. (b) Suzuki, A. *J. Organomet. Chem.* **1999**, *576*, 147. (c) Ishiyama, T.; Miyaura, N. *J. Organomet. Chem.* **2000**, *611*, 392. (d) Suzuki, A. In *Metal-Catalyzed Cross-Coupling Reactions*; Diederich, F., Stang, P. J., Eds.; Wiley-VCH: Weinheim, Germany, 1998; p 49.

(2) (a) Miyaura, N.; Yamada, K.; Suzuki, A. *Tetrahedron Lett.* **1979**, *20*, 3437. (b) Miyaura, N.; Yamada, K.; Suginome, H.; Suzuki, A. *J. Am. Chem. Soc.* **1985**, *107*, 972. (c) Miyaura, N.; Suzuki, A. *Org. Synth.* **1990**, *68*, 130. (d) Satoh, M.; Miyaura, N.; Suzuki, A. *Chem. Lett.* **1986**, 1329. (e) Miyaura, N.; Satoh, M.; Suzuki, A. *Tetrahedron Lett.* **1981**, *22*, 127.

(3) Goossen, L. J. *Chem. Commun.* **2001**, *7*, 669.

(4) (a) Goossen, L. J.; Ghosh, K. *Angew. Chem., Int. Ed.* **2001**, *40*, 3458. (b) Goossen, L. J.; Ghosh, K. *Eur. J. Org. Chem.* **2002**, *19*, 3254. (c) Goossen, L. J.; Winkel, L.; Döhring, A.; Ghosh, K.; Paetzold, J. *Synlett* **2002**, *8*, 1237. (d) Goossen, L. J.; Ghosh, K. *Chem. Commun.* **2001**, *20*, 2084.

(5) Kakino, R.; Camusi, S.; Shimizu, I.; Yamamoto, A. *Bull. Chem. Soc. Jpn.* **2002**, *75*, 137.

10.1021/om050685h CCC: $33.50
Publication on Web 12/02/2005

Scheme 3. Neutral and Anionic Pathways for Cross-Coupling Reactions

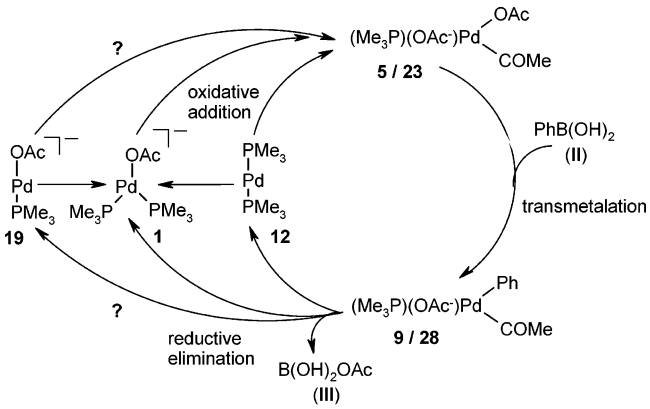

from boronic acids is itself of high synthetic interest.[4] In this model reaction, the acetate ion plays a triple role, as the leaving group, the base, and the counterion in the palladium(II) precursor, so that the overall number of possible intermediates is greatly reduced. The choice of such a simple model reaction enables us to evaluate multiple intertwined reaction pathways in a comprehensive manner.

In a preceding publication, we presented two viable catalytic cycles for this model reaction, one starting from a neutral Pd^0L_2 complex (**12**) and the other from a three-coordinate, anionic $[Pd^0L_2X]^-$ species (**1**) (Scheme 3).[6] According to calculations at the BP86/6-31G* level of theory, both the neutral and the anionic palladium(0) species lead to similar cycles, dominated by cis-configured four-coordinate intermediates. This was remarkable but not unexpected for the neutral pathway, as an increasing amount of evidence supports an initial formation of such cis- rather than trans-configured intermediates in cross-coupling reactions.[8] For the anionic pathway, our calculations support the intermediacy of the three-coordinate intermediates $[Pd(PMe_3)_2OAc]^-$, as proposed by Amatore and Jutand.[9,10] However, despite careful investigations, we could not find in our model systems any evidence for the existence of stable five-coordinate palladium(II) intermediates, which are currently believed to cause the profound effects of counterions on the performance of palladium catalysts. Instead, our calculations suggest that the higher catalytic activity of anionic complexes such as $[Pd(PMe_3)_2OAc]^-$ arises from their propensity to draw carbon electrophiles into their coordination sphere. This is in good accordance with calculations performed on the oxidative addition of aryl halides.[11]

Another important finding from our calculations[6] was that the transfer of an aryl group from the boronic acid to palladium appears to be feasible only if just one phosphine ligand is bound to palladium. While being compatible with earlier experimental results,[12] it remains to be seen whether this is a general feature of such transmetalation reactions.[13] If so, there are obvious implications for practical strategies in catalytic cross-coupling work.

These previous studies raise the question whether a third catalytic cycle, consisting solely of monophosphine complexes, would not altogether be more favorable, as one of the phosphine ligands must be liberated in any case for the transmetalation to occur (Scheme 3, outer cycle). Moreover, the isomer **23** of the initial oxidative addition product **5**, in which both acetate ligands are positioned trans to each other, has not been considered before,[6] although it might well lead to an advantageous transmetalation pathway. These issues are addressed in the present paper: starting from the coordinatively unsaturated anionic monophosphine complex **19**, new reaction pathways have been computed and cross-linked with the previously reported catalytic cycles, thus for the first time allowing a comprehensive comparison of neutral and anionic mono- and diphosphine palladium catalysts in a cross-coupling reaction.

Apart from our work,[6,11] there are several other recent computational studies that are relevant in the present context. Kozuch et al. have characterized active anionic zerovalent palladium catalysts by DFT calculations,[10] covering monodentate $[Pd(PR_3)_2X]^-$ and bidentate $[Pd\{R_2P(CH_2)_nPR_2\}X]^-$ species, and have explored the role of such anionic complexes (mostly with R = H, X = Cl) in the cross-coupling reaction $Ph{-}Cl + HS^- \rightarrow Ph{-}SH + Cl^-$, attributing the superiority of the anionic catalysts over the corresponding neutral species to the "flattening" of the energy landscape of the catalytic cycle.[14] One of the recent studies on palladium-catalyzed oxidative addition reactions[11,14−16] analyzes the mechanism of anion assistance (Pd vs $PdCl^-$ catalyst) in H−H, C−H, C−C, and C−Cl bond activation in terms of transition state interactions which are more stabilizing in the case of the anion.[15d] Finally, the role of the base in the transmetalation step of the Suzuki−Miyaura cross-coupling reactions has been investigated recently by DFT calculations on a model system containing $Pd(CH{=}CH_2)(PH_3)_2Br$ as the starting catalyst complex, $CH_2{=}CHB(OH)_2$ as the organoboronic acid, and OH^- as the base.[17] Our present work differs from these studies[14−17] by addressing a different and more complex model system and by covering several complete and competing catalytic cycles.

(6) Goossen, L. J.; Koley, D.; Hermann, H.; Thiel, W. *J. Am. Chem. Soc.* **2005**, *127*, 11102.

(7) (a) Nagayama, K.; Kawataka, F.; Sakamoto, M.; Shimizu, I.; Yamamoto, A. *Chem. Lett.* **1995**, 367. (b) Kakino, R.; Narahashi, H.; Shimizu, I.; Yamamoto, A. *Bull. Chem. Soc. Jpn.* **2002**, *75*, 1333. (c) Kakino, R.; Narahashi, H.; Shimizu, I.; Yamamoto, A. *Chem. Lett.* **1998**, 1143. (d) Juatnd, A.; Négri, S.; de Vries, J. G. *Eur. J. Inorg. Chem.* **2002**, 1711.

(8) (a) Casado, A. L.; Espinet, P. *J. Am. Chem. Soc.* **1998**, *120*, 8978. (b) Casado, A. L.; Espinet, P. *Organometallics* **1998**, *17*, 954. (c) Espinet, P.; Echavarren, A. M. *Angew. Chem., Int. Ed.* **2004**, *43*, 4704.

(9) (a) Amatore, C.; Jutand, A. *Acc. Chem. Res.* **2000**, *33*, 314. (b) Amatore, C.; Azzabi, M.; Jutand, A. *J. Am. Chem. Soc.* **1991**, *113*, 1670. (c) Amatore, C.; Jutand, A.; Suarez, A. *J. Am. Chem. Soc.* **1993**, *115*, 9531. (d) Amatore, C.; Jutand, A.; M'Barki, M. A. *Organometallics* **1992**, *11*, 3009. (e) Amatore, C.; Carré, E.; Jutand, A.; M'Barki, M. A.; Meyer, G. *Organometallics* **1995**, *14*, 5605.

(10) Kozuch, S.; Shaik, S.; Jutand, A.; Amatore, C. *Chem. Eur. J.* **2004**, *10*, 3072.

(11) (a) Goossen, L. J.; Koley, D.; Hermann, H.; Thiel, W. *Chem. Commun.* **2004**, 2141. (b) Goossen, L. J.; Koley, D.; Hermann, H.; Thiel, W. *Organometallics* **2005**, *24*, 2398.

(12) Louie, J.; Hartwig, J. F. *J. Am. Chem. Soc.* **1995**, *117*, 11598.

(13) (a) Farina, V.; Krisnan, B. *J. Am. Chem. Soc.* **1991**, *113*, 9585. (b) Farina, V.; Roth, G. P. *Adv. Met.-Org. Chem.* **1996**, *5*, 1. (c) Amatore, C. Bahsoun, A.; Jutand, A, Meyer, G.; NdediNtepe, A.; Ricard, L. *J. Am. Chem. Soc.* **2003**, *125*, 4212.

(14) Kozuch, S.; Amatore, C.; Jutand, A.; Shaik, S. *Organometallics* **2005**, *24*, 2319.

(15) (a) Bickelhaupt, F. M.; Ziegler, T.; Schleyer, P. v. R. *Organometallics* **1995**, *14*, 2288. (b) Diefenbach, A.; Bickelhaupt, F. M. *J. Chem. Phys.* **2001**, *115*, 4030. (c) de Jong, G. T.; Sola, M.; Visscher, L.; Bickelhaupt, F. M. *J. Chem. Phys.* **2004**, *121*, 9982. (d) Diefenbach, A.; de Jong, G. T.; Bickelhaupt, F. M. *J. Chem. Theor. Comput.* **2005**, *1*, 286.

(16) (a) Senn, H. M.; Ziegler, T. *Organometallics* **2004**, *23*, 2980. (b) Sundermann, A.; Uzan, O.; Martin, J. M. L. *Chem. Eur. J.* **2001**, *7*, 1703. (c) Albert, K.; Gisdakis, P.; Rösch, N. *Organometallics* **1998**, *115*, 4030. (d) Reinhold, M.; McGrady, J. E.; Perutz, R. N. *J. Am. Chem. Soc.* **2004**, *126*, 5268.

(17) Braga, A. A. C.; Morgon, N. H.; Ujaque, G.; Maseras, F. *J. Am. Chem. Soc.* **2005**, *127*, 9298.

Scheme 4. Anionic Catalytic Cycles

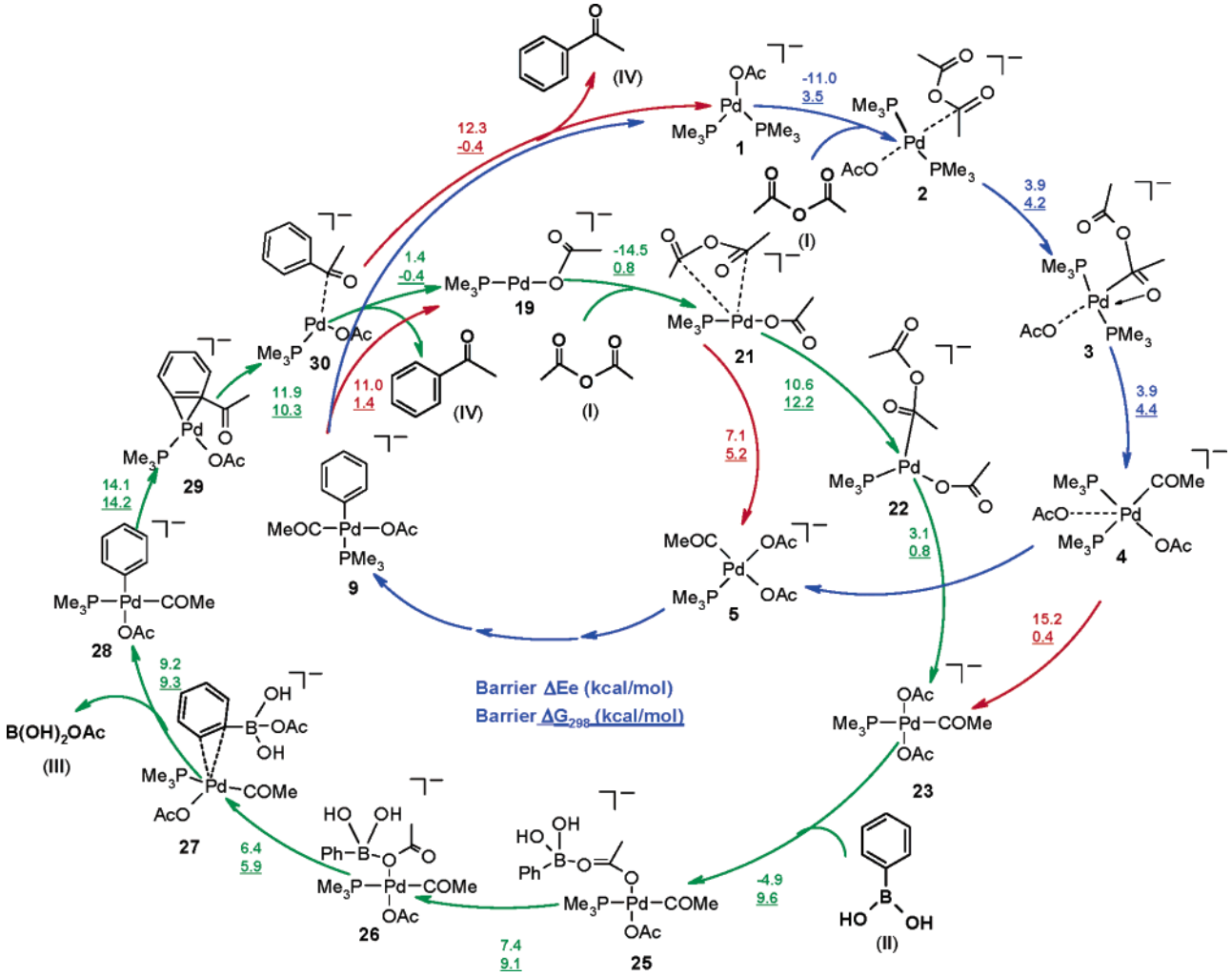

2. Computational Details

All calculations were performed with the Gaussian98 and Gaussian03 suites of programs.[18] The DFT calculations employed the BP86 functional[19,20] using the standard 6-31G* basis[21] for all atoms, except for palladium, which was described by the LANL2DZ valence basis set in combination with the corresponding effective core potential.[22] Geometries were fully optimized, normally without symmetry constraints. Harmonic force constants were computed at the optimized geometries to characterize the stationary points as minima or saddle points. Zero-point vibrational corrections were determined from the harmonic vibrational frequencies to convert the total energies E_e to ground-state energies E_0. The rigid-rotor harmonic-oscillator approximation was applied for evaluating the thermal and entropic contributions that are needed to derive the enthalpies H_{298} and Gibbs free enthalpies G_{298} at 298 K. Transition states were located from a linear transit scan in which the reaction coordinate was kept fixed at different distances while all other degrees of freedom were optimized. After the linear transit search the transition states were optimized using the default Berny algorithm implemented in the Gaussian code.[18] In critical cases, the nature of a given transition state was analyzed by IRC (intrinsic reaction coordinate) computations.

For further validation, single-point BP86 calculations were performed at the optimized BP86/6-31G* geometries employing larger basis sets (EXT): palladium was described by Stuttgart−Dresden quasirelativistic pseudopotentials and the associated (8s7p5d)/[6s5p3d] valence basis set;[23] the 6-31+G* basis was employed for O, P, B, and C and the 6-31G** basis for all H atoms[21] (which will be abbreviated as BP86/EXT). Single-point solvent calculations were performed at the optimized gas-phase geometries for all the intermediates and transition states, using the CPCM[24] approach, which is an implementation of the conductor-like screening solvation model (COSMO)[25] in Gaussian03; THF was used as solvent (dielectric constant $\epsilon = 7.58$) with UAHF (united atom Hartree−Fock) radii for the respective atoms (Pd, H, B, C, O, P). The charge distribution around the metal center was analyzed using Weinhold's NPA (natural population analysis) approach.[26]

3. Results

A. Outline of the Catalytic Cycles. The general features of the calculated anionic cycles are summarized in Scheme 4. For

(18) Frisch, M. J., et al. *Gaussian 03*, revision B.05; Gaussian, Inc., Pittsburgh, PA, 2003.
(19) Becke, A. D. *Phys. Rev. A* **1988**, *33*, 3098.
(20) Perdew, J. P. *Phys. Rev. B* **1986**, *33*, 8822.
(21) Hehre, W. J.; Radom, L.; Schleyer, P. v. R.; Pople, J. A. *Ab Initio Molecular Orbital Theory*; Wiley: New York, 1986; p 65.
(22) Hay, P. J.; Wadt, W. R. *J. Chem. Phys.* **1985**, *82*, 299.
(23) Andrae, D.; Häussermann, U.; Dolg, M.; Stoll, H.; Preuss, H. *Theor. Chim. Acta* **1990**, *77*, 123.
(24) (a) Barone. V.; Cossi, M. *J. Phys. Chem. A* **1998**, *102*, 1995. (b) Cossi, M.; Rega, N.; Scalmani, G.; Barone, V. *J. Comput. Chem.* **2003**, *24*, 669.
(25) Klamt, A.; Schüürmann, G. *J. Chem. Soc., Perkin Trans 2* **1993**, 799. (b) Schäfer, A.; Klamt, A.; Sattel, D.; Lohrenz, J. C. W.; Eckert, F. *Phys. Chem. Chem. Phys.* **2000**, *2*, 2187.
(26) (a) Reed, A. E.; Curtiss, L. A.; Weinhold, F. *Chem. Rev.* **1988**, *88*, 899. (b) Glendening, E. D.; Reed, A. E.; Carpenter, J. E.; Weinhold, F. NBO Version 3.1.

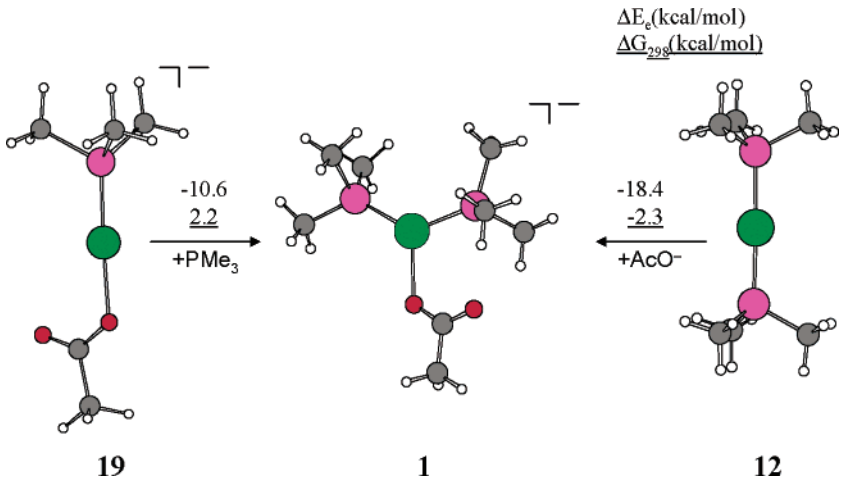

Figure 1. Energetics for interconversion between the palladium(0) catalysts considered presently.

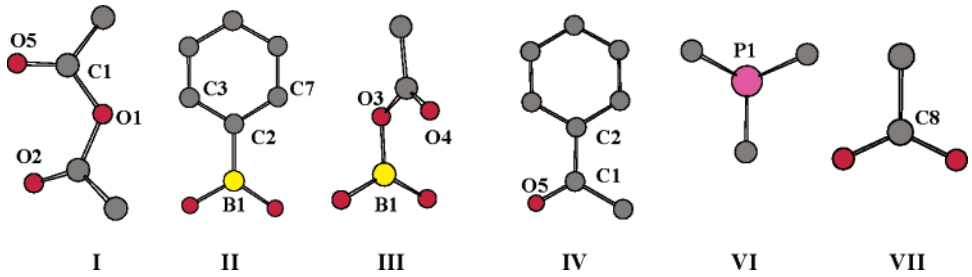

Figure 2. Starting materials and products. BP86/6-31G* optimized structures are shown, with hydrogens removed for clarity. Color code: C, gray; O, red; B. yellow; P, violet.

convenience, the numbering of the intermediates has been chosen to be consistent with our preceding paper.[6] The previously discussed cycle **1** → **5** → **9** → **1** and the presently computed cycle **19** → **23** → **28** → **19** are represented by blue and green arrows, respectively, while the interconnections are indicated by red arrows in Scheme 4. Due to these interconnections, oxidative addition of acetic anhydride to **1** or **19** can lead in each case to the formation of either **5** or **23**, which are starting points of transmetalation sequences where the acyl and phosphine ligands remain cis (**5** → **9**) or trans (**23** → **28**) to each other. In the final reductive elimination, both **9** and **28** can be converted into either **1** or **19**.

Figure 1 shows the anionic monophosphine complex **19**, the anionic "Amatore−Jutand-type" diphosphine complex **1**, and the neutral $Pd(PMe_3)_2$ molecule **12**, which all serve as starting points for the catalytic cycles considered in this and previous studies.[6] The computed relative free energies are similar (Figure 1), confirming that each of these species can be involved in catalysis.[27] The geometries of **1** and **12** have already been reported.[6] In both anionic complexes, the acetate is coordinated in a monodentate fashion, with the Pd−O bond in **1** being much longer than in **19** (2.327 vs 2.131 Å). Compound **19** has a linear geometry; the Pd−P bond distance is shorter than in the other complexes (2.161 Å in **19** vs 2.247 Å in **1** and 2.292 Å in **12**).

The geometries and energies of all starting materials and products, namely acetic anhydride **I**, phenylboronic acid **II**, boric acid adduct **III**, acetophenone **IV**, trimethylphosphine **VI**, and acetate **VII** (Figure 2), have also been reported previously.[6]

(27) Adding a bare metal counterion (K^+) in the calculation of the anion **1** leads to dissociation into the corresponding neutral palladium species and the metal acetate. Such a gas-phase description is not realistic, however, because the ions will be solvated under the experimental conditions, and counterions are therefore not included in this work.

In the calculation of the catalytic cycles, we have evaluated for each segment, i.e. oxidative addition, transmetalation, and reductive elimination, the changes in electronic energy (ΔE_e) and Gibbs free energy (ΔG_{298}) at the optimized gas-phase geometries. The BP86/6-31G* results were validated by calculating single-point energies of the resulting intermediates and transition states with a larger basis set (ΔE_{EXT}). Finally, a solvent field was applied to account for solvent effects (ΔE_{sov}). The figures that display energy profiles for reaction steps will show these four quantities.

B. Oxidative Addition and Ligand Exchange Starting from the Anionic Monosphosphine Complex 19. According to our calculations, the approach of a molecule of acetic anhydride (**I**) to the monophosphine complex $[Pd(PMe_3)OAc]^-$ (**19**) directly leads to the adduct **20** in an exothermic reaction (ΔE_e = −14.5 kcal/mol, ΔG_{298} = 0.8 kcal/mol). In this intermediate, the acetic anhydride is located about 3.5 Å from the palladium center (Pd(1)−C(1) = 3.640 Å, Pd(1)−C(8) = 3.608 Å) and is oriented perpendicular to the P−Pd−O(4) plane (Figure 3). The stability of this adduct results from gas-phase interactions of C−H groups of the acetic anhydride with the two oxygen atoms (O(4) and O(3)) of the catalyst fragment (Figure 3). A certain charge transfer from the acetic anhydride to the metal center (Pd(1) = −0.236 e in **20** vs −0.195 e in **19**) can be observed. In **20**, the C(8) atom is slightly closer to the palladium center than C(1) (Pd(1)−C(8) = 3.608 Å, Pd(1)−C(1) = 3.640 Å). Further shortening of the Pd(1)−C(8) bond initiates the strongly exothermic (ΔE_e = −12.0 kcal/mol, ΔG_{298} = −12.8 kcal/mol) oxidative addition of acetic anhydride to the palladium center under formation of the square-planar palladium(II) complex **5b**, in which the two acetyl groups are located cis to each other (Figure 3). The reaction requires only moderate activation (ΔE_e = 7.1 kcal/mol, ΔG_{298} = 5.2 kcal/mol). In the transition state **[20-5b]**‡ the P−Pd−O(4) angle is decreased by 22.5° in

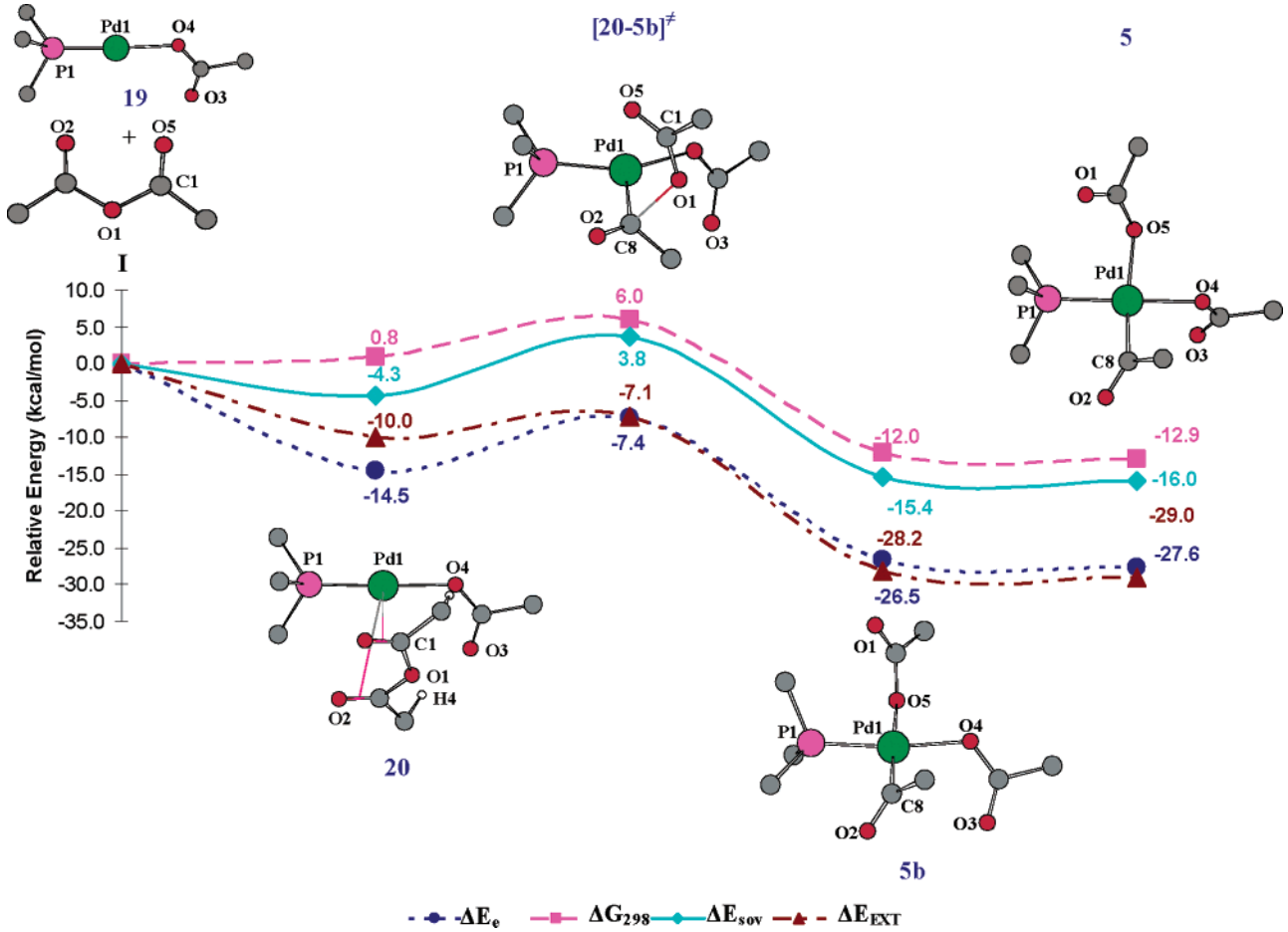

Figure 3. Energy profile for the conversion from **19** → **5**. For the conventions, see Figure 2.

Table 1. Optimized Geometric Parameters for Complexes Involved in the Oxidative Addition Process 19 → 5[a]

compd	Pd−P(1)	Pd−C(1)	Pd−O(1)	Pd−O(2)	Pd−O(3)	Pd−O(4)	Pd−O(5)	P−Pd−O(4)
19	2.161				3.307	2.131		176.8
20	2.178	3.640	3.550	3.951	3.329	2.141	4.173	174.4
[20−5b]≠	2.255	3.227/2.027[b]	2.850	2.899	3.411	2.164	3.019	151.9
5b	2.274	3.182/1.988[b]	3.546	2.877	3.323	2.120	2.254	171.5

[a] Bond distances are provided in angstroms and bond angles in degrees. [b] Pd(1)−C(1)/Pd(1)−C(8).

comparison to **20**, the Pd(1)−C(8) bond is shortened to 2.027 Å, and the C(8)−O(1) bond is elongated to 2.087 Å. The transition vector (72 *i*cm^{-1}) reflects a further shortening of the Pd(1)−C(8) bond with a concomitant elongation of the C(8)−O(1) bond.

In the oxidative addition product **5b**, the C(8)−O(1) bond is completely cleaved, the Pd(1)−C(8) bond is further shortened to 1.988 Å, and the Pd(1)−O(1) distance amounts to 3.546 Å. A slight rearrangement of this intermediate leads to the formation of the energetically almost degenerate isomer **5** (ΔE_e = −1.1 kcal/mol, ΔG_{298} = −0.9 kcal/mol). As discussed before,[6] **5** is accessible also from the three-coordinate palladium(0) species **1** and is a good starting point for a transmetalation reaction leading to the aryl−Pd species **9**.

The overall reaction profile obtained after basis set extension (see Computational Details) is almost identical with that calculated with the 6-31G* basis set (ΔE_{EXT} vs ΔE_e, Figure 3). This confirms the suitability of the chosen basis set for these reactions.[15c] Gratifyingly, the calculated energies within a THF solvent field (see Computational Details) also show a trend similar to that for the gas-phase electronic energies. We have performed such additional calculations for all subsequent reaction steps (see Figures 4−9), but we will not discuss them unless they differ significantly from the standard gas-phase BP86/6-31G* results.

The structural parameters of all intermediates and transition states involved in the oxidative addition/ligand exchange sequence displayed in Figure 3 are summarized in Table 1. Selected NPA charges (Table S3) and more detailed structural data are available in the Supporting Information.

Alternatively, the oxidative addition reaction might also proceed such that, instead of **5**, its isomer **23** is formed, in which the acetyl groups are not located cis but trans to each other. As can be seen from Figure 4, such a pathway can indeed be found, but it requires several additional intermediates and appears to be energetically not quite as favorable.

The branching from the preceding pathway takes place after the formation of the initial adduct **20**, which can be converted into the almost degenerate isomer **21** (ΔE_e = −0.4 kcal/mol, ΔG_{298} = −2.4 kcal/mol) by a slight rotation of the acetic anhydride fragment. An important structural feature of **21** is the presence of two C−H interactions from the acetic anhydride fragment to the metal center and O(4) (C−H(4) = 1.129 Å and C−H(5) = 1.123 Å). These gas-phase interactions are also manifested by elongated Pd(1)−C(1) and Pd(1)−C(8) distances (Pd(1)−C(1) = 4.402 Å and Pd(1)−C(8) = 4.470 Å).

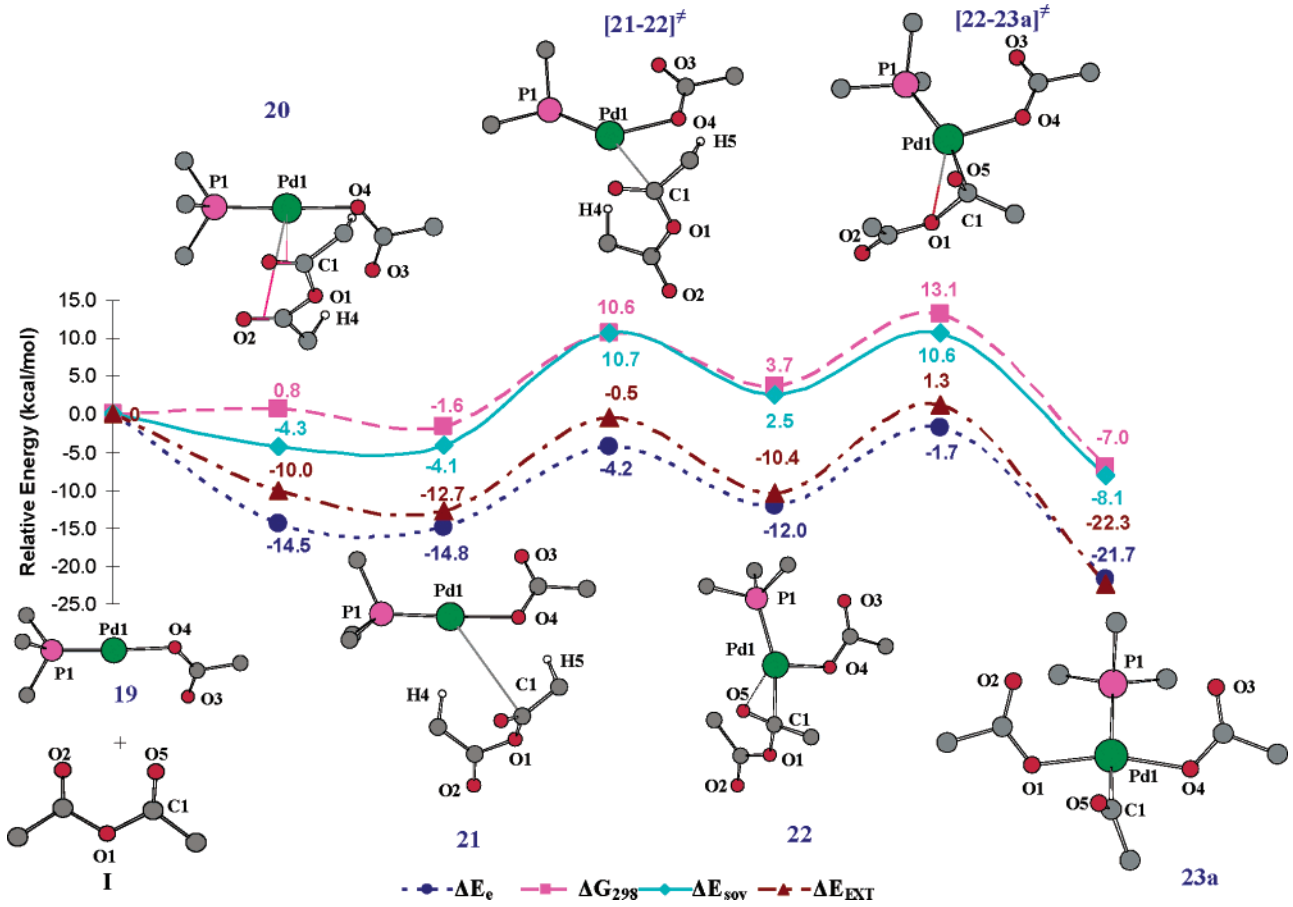

Figure 4. Energy profile for the conversion from **19** → **23a**. For the conventions, see Figure 2.

Table 2. Optimized Geometric Parameters for Complexes Involved in the Oxidative Addition Process 19 → 23[a]

compd	Pd−P1	Pd−C1	Pd−O1	Pd−O2	Pd−O3	Pd−O4	Pd−O5	P−Pd−O4
21	2.175	4.402	4.493	5.425	3.164	2.159	4.779	177.6
[21-22]≠	2.209	2.853	3.552	5.125	3.249	2.223	2.652	130.4
22	2.351	2.089	3.093	4.787	3.405	2.179	2.214	105.7
[22-23a]≠	2.352	2.086	2.486	4.122	3.407	2.214	2.672	108.8
23a	2.481	1.997	2.124	3.286	3.342	2.133	2.864	96.2

[a] Bond distances are provided in angstroms and bond angles in degrees.

Gradual approach of the less distant C(1) toward the palladium center leads to the formation of another adduct **22**. In comparison to the previous route (Figure 3), the activation barrier of this additional rearrangement is rather high (ΔE_e = 10.6 kcal/mol, ΔG_{298} = 12.2 kcal/mol). In the transition state **[21-22]**≠, which was validated by an IRC calculation, the Pd(1)−C(1) distance is significantly shortened (Pd(1)−C(1) = 2.853 Å), the P−Pd−O(4) angle has decreased to 130.4°, and the C(1)−O(5) distance is slightly elongated (C(1)−O(5) = 1.231 vs 1.209 Å in **I**). The transition vector of **[21-22]**≠ (80*i* cm^{-1}) represents the approach of C(1) toward Pd(1).

The product **22** can be seen as a π complex of the acetic anhydride, as the C(1)−O(5) bond coordinates to palladium in an η^2 fashion (Pd(1)−C(1) = 2.089 Å, Pd(1)−O(5) = 2.214 Å). The C(1)−O(5) bond length of 1.290 Å is much larger than in free acetic anhydride (1.209 Å). NBO analysis suggests a bonding interaction between the occupied π_b C(1)−O(5) orbital and an unoccupied palladium orbital and a strong back-donation from the occupied d orbital of palladium to the unoccupied π^* C(1)−O(5) orbital. Overall, the conversion **21** → **22** is accompanied by a net electron transfer of ca. 0.4 e from palladium to the C(1)−O(5) moiety (see NPA charges in Table S4; Supporting Information).

Decreasing the Pd(1)−O(1) distance in **22** initiates the actual oxidative addition of the acetic anhydride that leads to the formation of complex **23a**. This process is again strongly exothermic (ΔE_e = −9.7 kcal/mol, ΔG_{298} = −10.7 kcal/mol) but has a significant activation energy (ΔE_e = 10.3 kcal/mol, ΔG_{298} = 9.4 kcal/mol). In the corresponding transition state **[22-23a]**≠, the Pd(1)−O(1) distance of 2.486 Å and the C(1)−O(5) distance of 1.245 Å are shorter while the C(1)−O(1) distance of 1.620 Å is slightly longer than in **22**. The imaginary frequency (37 *i*cm^{-1}) shows the formation of the Pd(1)−O(1) bond with simultaneous elongation of the C(1)−O(1) bond.

The product of the oxidative addition **23a** is again a square-planar palladium(II) complex (Figure 4), but in contrast to **5**, the two acetates are now located trans to each other. The oxidative nature of this reaction sequence is reflected in an increase of the NPA charge on palladium from −0.195 e in **19** to 0.466 e in **23a** (Table S4) and a decrease of the NPA charges on the new ligand atoms, in particular on C(1) (from 0.799 e to 0.395 e). **23a** is easily converted into its rotamer **23**, which is a good starting point for a transmetalation sequence (see below).

The structural parameters of all intermediates and transition states involved in the oxidative addition/ligand exchange sequence displayed in Figure 4 are summarized in Table 2.

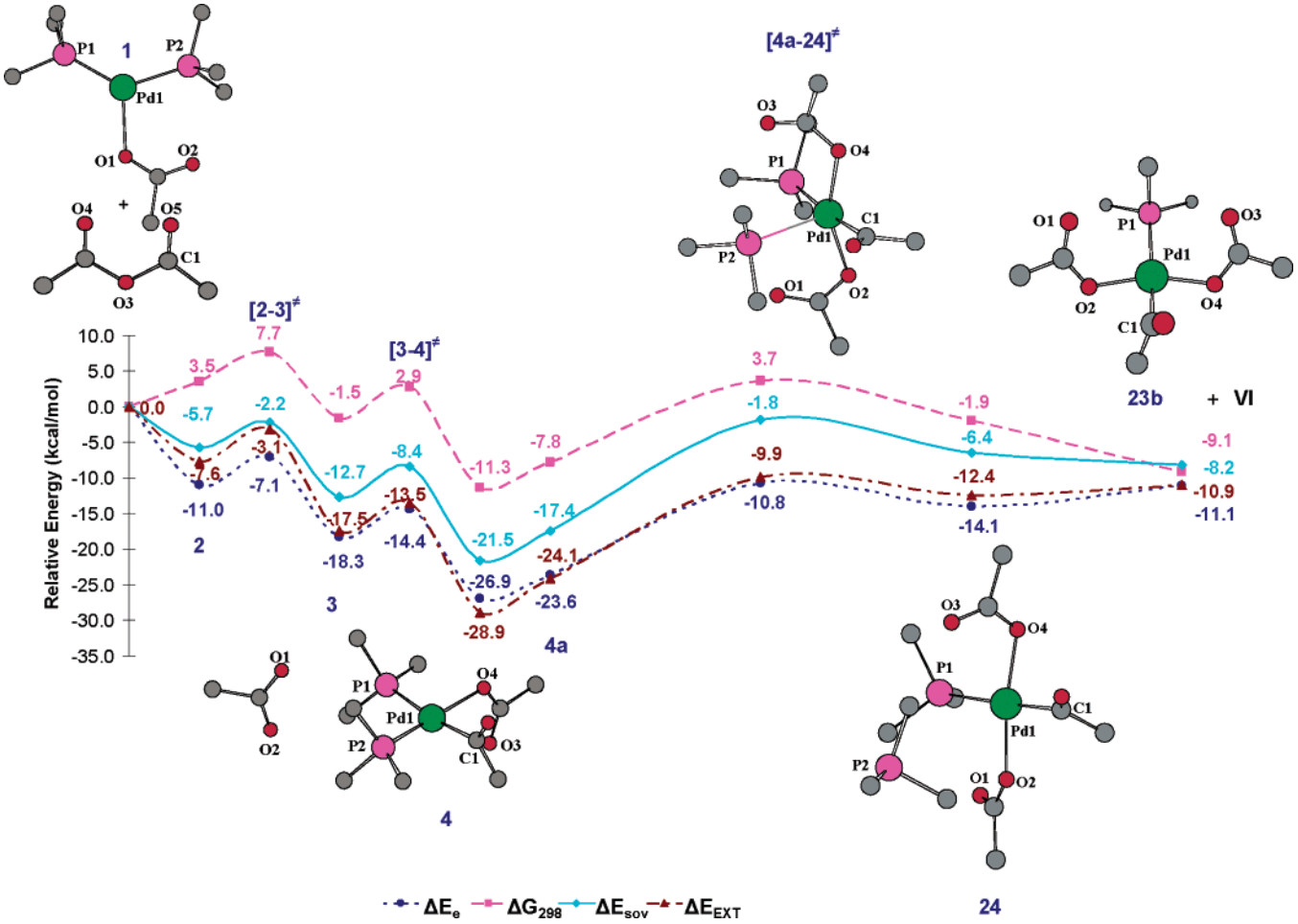

Figure 5. Energy profile for the oxidative addition starting from $[Pd(PMe_3)_2OAc]^-$ (**1**) to **23**. For the conventions, see Figure 2. Steps **1** → **4a** have been discussed elsewhere.[6]

Table 3. Optimized Geometric Parameters for Complexes Involved in the Oxidative Addition Process 1 → 23[a]

compd	Pd−P1	Pd−P2	Pd−C1	Pd−O1	Pd−O2	Pd−O3	Pd−O4	Pd−O5	P1−Pd−O4
4a	2.459	2.285	2.031	4.226	3.162	3.195	2.195	2.967	87.5
[4a-24]≠	2.467	2.808	1.992	3.335	2.199	3.333	2.191	2.895	96.0
24	2.478	4.926	2.000	3.376	2.144	3.141	2.129	2.877	91.9
23b	2.481		1.997	3.342	2.137	3.286	2.125	2.864	97.1

[a] Bond distances are provided in angstroms and bond angles in degrees.

Selected NPA charges (Table S4) and more detailed structural data are available in the Supporting Information.

C. Oxidative Addition Starting from the Anionic Bisphosphine Complex 1. We have previously reported that a feasible pathway for the oxidative addition of acetic anhydride to complex **1** leads to the formation of the intermediate **5**, in which both acetyl ligands are positioned cis to each other (see Scheme 4, blue arrows).[6] Although this reaction sequence is energetically favorable, one must also consider an alternative route, in which the acetic anhydride adds in a different manner to yield isomer **23**, in which the two acetyl ligands are located trans to each other.

This alternative pathway is entered from the previously discussed[6] intermediate **4a** if $P(2)Me_3$ (rather than the less strongly bound $P(1)Me_3$ ligand) is moved away from the palladium center. Thereby intermediate **24** is formed in an endothermic reaction ($\Delta E_e = 9.5$ kcal/mol, $\Delta G_{298} = 5.9$ kcal/mol) that requires only moderate activation ($\Delta E_e = 12.8$ kcal/mol, $\Delta G_{298} = 11.5$ kcal/mol).

The transition state **[4a-24]‡** has a trigonal-bipyramidal geometry with the acyl group and the phosphines in equatorial positions (Pd−P(1)−P(2)−C(1) = 178.9°), and the oxygen atoms O4 and O2 of the acetyl ligands occupying the axial positions. The Pd(1)−P(2) distance is significantly increased (2.808 Å in **[4a-24]‡** vs 2.285 Å in **4a**) while the Pd(1)−O(2) distance is much reduced (2.199 Å in **[4a-24]‡** vs 3.162 Å in **4a**). The transition vector (33 $i$cm^{-1}) reflects the removal of the $P(2)Me_3$ fragment from the metal center (Figure 5).

In the product **24**, the phosphine has almost left the coordination sphere of the palladium (Pd−P(2) = 4.926 Å) while the acetyl group is now strongly bound (Pd−O(2) = 2.144 Å). A complete removal of the weakly bound phosphine from **24** is easily achieved, affording the oxidative addition product **23b** ($\Delta E_e = 3.0$ kcal/mol, $\Delta G_{298} = -7.2$ kcal/mol). Only a minor conformational rearrangement of **23b** is needed to yield the isomeric complex **23** ($\Delta E_e = -0.5$ kcal/mol, $\Delta G_{298} = -1.8$ kcal/mol), which is a suitable starting point for the transmetalation process (see below).

The structural parameters of all intermediates and transition states involved in the oxidative addition/ligand exchange sequence displayed in Figure 5 are summarized in Table 3.

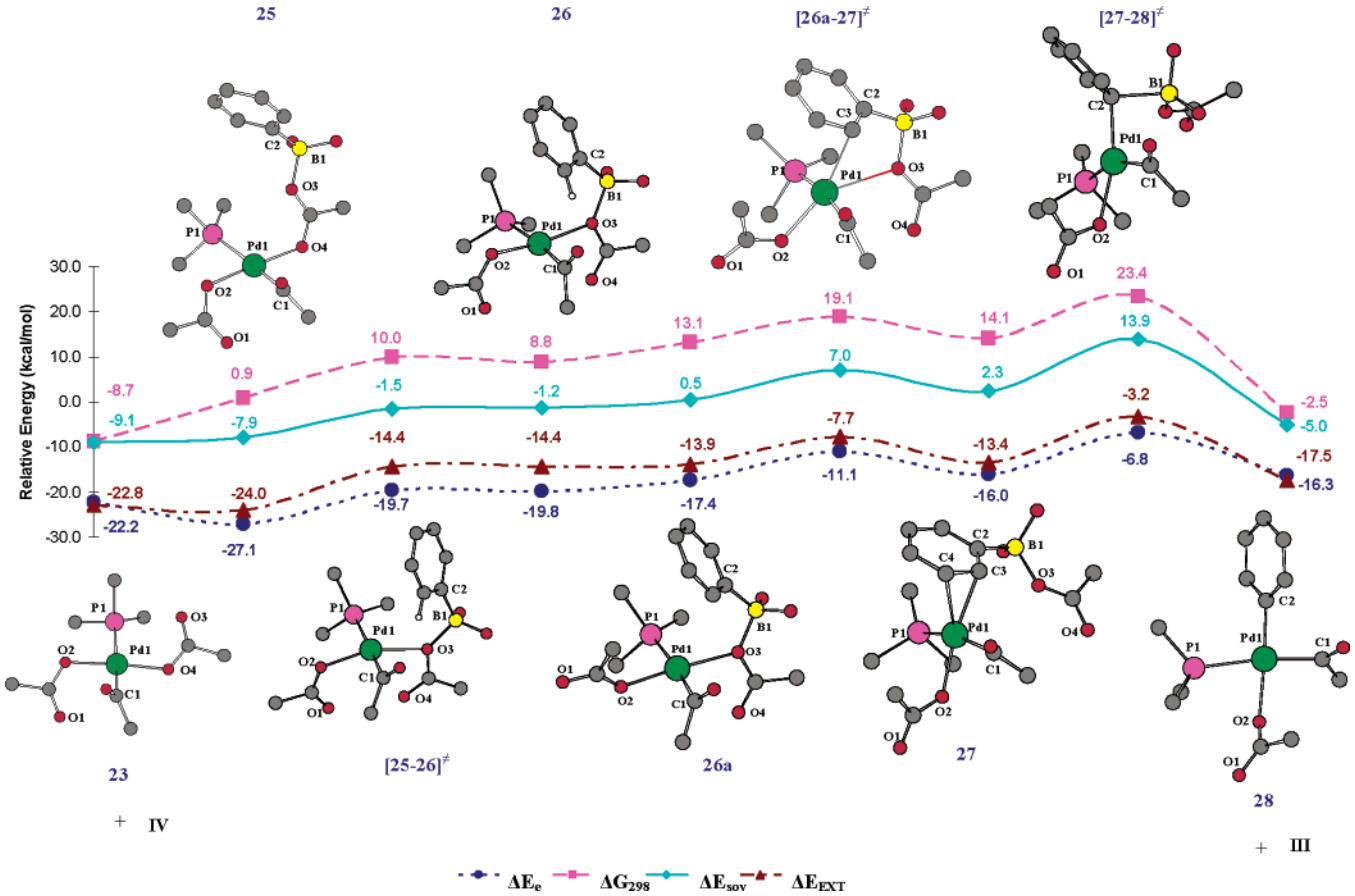

Figure 6. Energy profile for the transmetalation process **23** → **28**. For the conventions, see Figure 2. The energy scale refers to Figure 4.

Table 4. Optimized Geometric Parameters for Complexes Involved in the Transmetalation Sequence 23 → 28[a]

compd	Pd−P1	Pd−C1	Pd−C2	Pd−O1	Pd−O2	Pd−O3	Pd−O4	C2−B1	P−Pd−O2
23	2.483	1.993		3.221	2.124	3.329	2.139		86.8
25	2.484	1.992	5.282	3.212	2.119	3.281	2.159	1.631	83.2
[25-26]≠	2.455	1.983	5.282	3.167	2.167	2.425	2.732	1.631	93.2
26	2.459	1.991	3.590	3.197	2.155	2.322	2.876	1.624	92.7
26a	2.475	1.995	3.432	4.244	2.117	2.277	2.931	1.624	84.3
[26a-27]≠	2.501	1.989	3.082	4.255	2.175	2.793	3.696	1.630	86.8
27	2.543	2.007	3.122	4.238	2.154	3.630	4.677	1.642	80.0
[27-28]≠	2.541	2.016	2.159	4.248	2.172	3−127	4.919	2.016	77.8
28	2.465	2.014	2.033	4.244	2.209				77.9

[a] Bond distances are provided in angstroms and bond angles in degrees.

Selected NPA charges (Table S5) and more detailed structural data are available in the Supporting Information.

D. An Alternative Transmetalation Pathway. The finding that the oxidative addition of acetic anhydride to palladium(0) species can also lead to complexes with the acyl and the phosphine ligand oriented trans to each other (**23a**,**b**) raises the possibility that the latter might also serve as suitable starting points for transmetalation reactions, like the isomeric cis complex **5**. We have indeed found a viable reaction pathway for the transfer of an aryl group from boronic acid starting from compound **23**, which is accessible from compounds **23a**,**b** (Figures 4 and 5) just via slight rotation of one of the acetate ligands (Figure 6).

The approach of a molecule of phenylboronic acid **II** leads to an exothermic coordination of the Lewis acidic boron center to the sp^2-hybridized O(3) atom, giving rise to intermediate **25** ($\Delta E_e = -4.9$ kcal/mol, $\Delta G_{298} = 9.6$ kcal/mol). The Pd(1)−O(3) and Pd(1)−O(4) distances in this adduct amount to 3.281 and 2.159 Å, respectively. Gradual decrease of the Pd(1)−O(3) distance then affords the intermediate **26**, in which the boron and the palladium both coordinate to O(3). Reaching the corresponding transition state **[25-26]≠** requires only moderate activation ($\Delta E_e = 7.4$ kcal/mol, $\Delta G_{298} = 9.1$ kcal/mol). Its geometry is already closely related to that of the product **26**, and the transition vector (49 $i$cm^{-1}) represents the incoming of O(3) to Pd(1) and concomitant lengthening of the Pd(1)−O(4) σ bond. This reaction pathway was validated by an IRC calculation.

During the rearrangement from **25** to **26**, the phenyl moiety moves closer to the palladium center, so that the Pd(1)−C(2) distance decreases from 5.282 to 3.590 Å. A slightly endothermic rotation of one of the acetate ligands with formation of intermediate **26a** sets the stage for the following coordination of the phenyl group ($\Delta E_e = 2.3$ kcal/mol, $\Delta G_{298} = 4.4$ kcal/mol). In structure **26a**, the sp^2 O(1) atom is positioned further away from palladium and the O(1)−O(2)−Pd angle is significantly increased (153.7 vs 91.9° in **26**). Decreasing the Pd(1)−C(2) distance in **26a** then leads to the formation of intermediate **27**, in which the C(3)−C(4) phenyl double bond is coordinated to the palladium in an η^2 fashion (Pd(1)−C(3) = 2.328 Å, Pd-

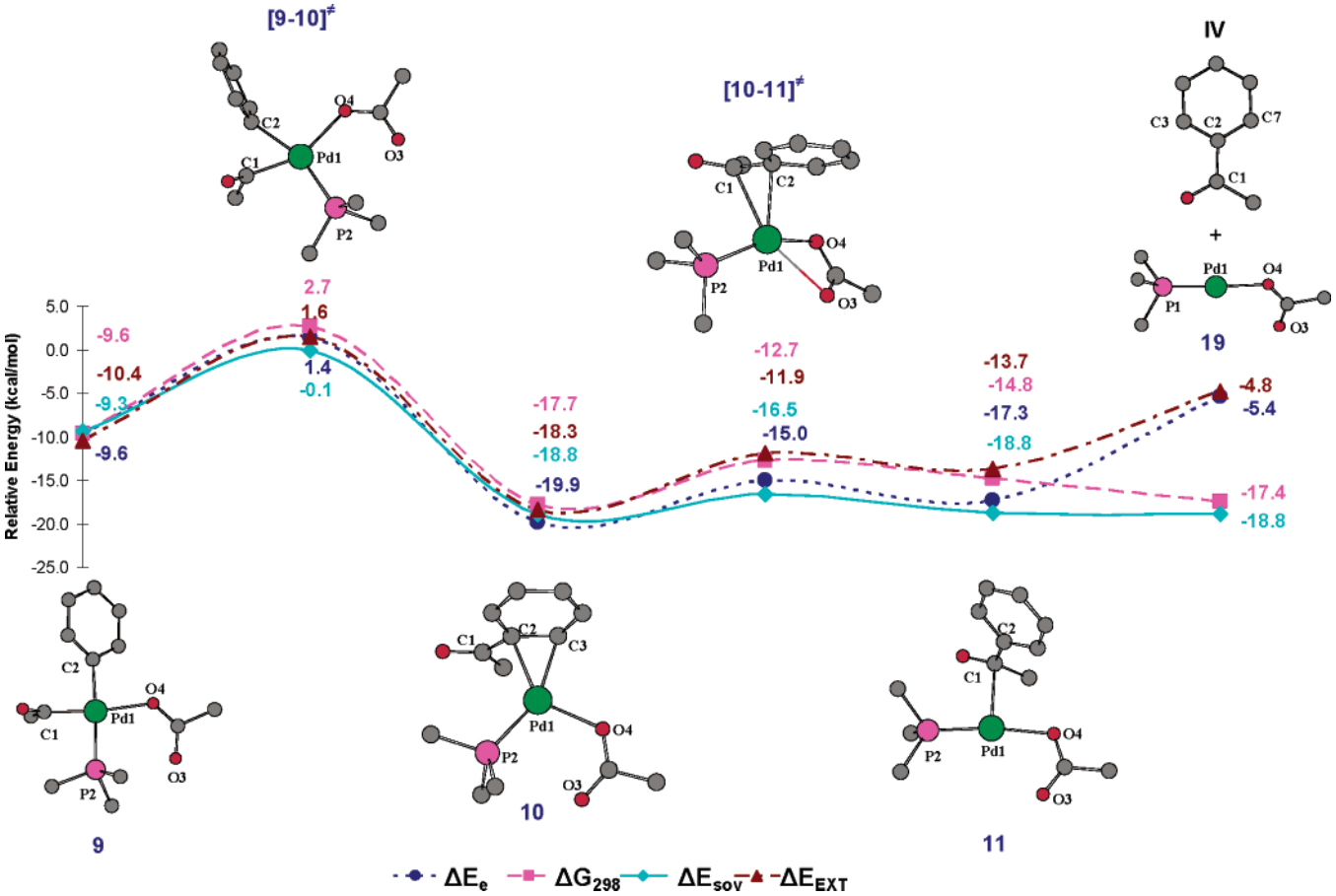

Figure 7. Energy profile for the reductive elimination from intermediate **9** to **19**. For the conventions, see Figure 2. See ref 6 for a discussion of the first two steps.

(1)−C(4) = 2.425 Å). The formation of such π-complexes is common in palladium chemistry, as such intermediates are also found in oxidative addition reactions of aryl halides with palladium(0) complexes.[16] The corresponding transition state **[26a-27]**$^{\neq}$, which was validated by an IRC calculation, has a small activation barrier (ΔE_e = 6.4 kcal/mol, ΔG_{298} = 5.9 kcal/mol). Its imaginary mode (55 *i*cm^{-1}) involves the coordination of the phenyl moiety to palladium and a simultaneous elongation of the Pd(1)−O(3) bond. In **[26a-27]**$^{\neq}$, the C(3) atom of the phenyl group is already very close to the palladium center (C(3)−Pd(1) = 2.547 Å), while the Pd(1)−O(3) bond is almost cleaved (Pd(1)−O(3) = 2.793 Å; Table 4).

Simultaneous shortening of the Pd(1)−C(2) distance and lengthening of the C(2)−B(1) distance in **27** initiates the actual transfer of the phenyl group, leading to intermediate **28** via the transition state **[27-28]**$^{\neq}$. This reaction step, which leads to a complete removal of the $B(OH)_2OAc$ (**III**) fragment, requires only a moderate activation energy (ΔE_e = 9.2 kcal/mol, ΔG_{298} = 9.3 kcal/mol). In the transition state **[27-28]**$^{\neq}$, the C(2)−B(1) bond is already stretched to 2.016 Å (Table 4) and the C(2) atom is within bonding distance to the palladium (Pd(1)−C(2) = 2.159 Å). The main component of the transition vector (320 *i*cm^{-1}) represents the elongation of the C(2)−B(1) bond. The transmetalated product **28** has an almost square-planar geometry, with the aryl and the acyl group located cis to each other. It is ideally suited for the reductive elimination sequence outlined in the following section.

The structural parameters of all intermediates and transition states involved in the transmetalation/ligand exchange sequence are summarized in Table 4. Selected NPA charges (Table S6) and more detailed structural data are available in the Supporting Information.

E. Reductive Elimination under Formation of the Anionic Monophosphine Complex 19. To close the alternative catalytic cycle, a reductive elimination pathway has to be identified that allows the conversion of compound **9** back to the anionic two-coordinate species **19**. In our preceding work we have shown that the reductive elimination of acetophenone from intermediate **9** may result in the formation of the anionic three-coordinate species **1** and the neutral Pd^0L_2 species **12**. We now found that the anionic two-coordinate species **19** is also accessible via this established route (for details see ref 6): a two-step rearrangement of **9** leads to the formation of compound **11**, in which the acetophenone is only loosely bound by an interaction of the electrophilic carbonyl carbon with the electron-rich palladium center (Figure 7).

With intermediate **11** as the starting material, substitution of acetophenone by phosphine yields **1**, as shown previously.[6] However, if no phosphine is provided, the two-coordinate anionic complex **19** can be formed directly by dissociation of acetophenone. This final reaction step is quite facile (ΔE_e = 11.9 kcal/mol, ΔG_{298} = −2.6 kcal/mol). One can thus imagine that it will depend on the reaction conditions, i.e., the concentration of phosphine in solution, which of the coordinatively unsaturated palladium(0) species **1** and **19** is regenerated after completion of the catalytic cycle. At this point a crossover between the different pathways can easily occur.

A viable route for the reductive elimination of acetophenone was also found when starting from intermediate **28**, the end

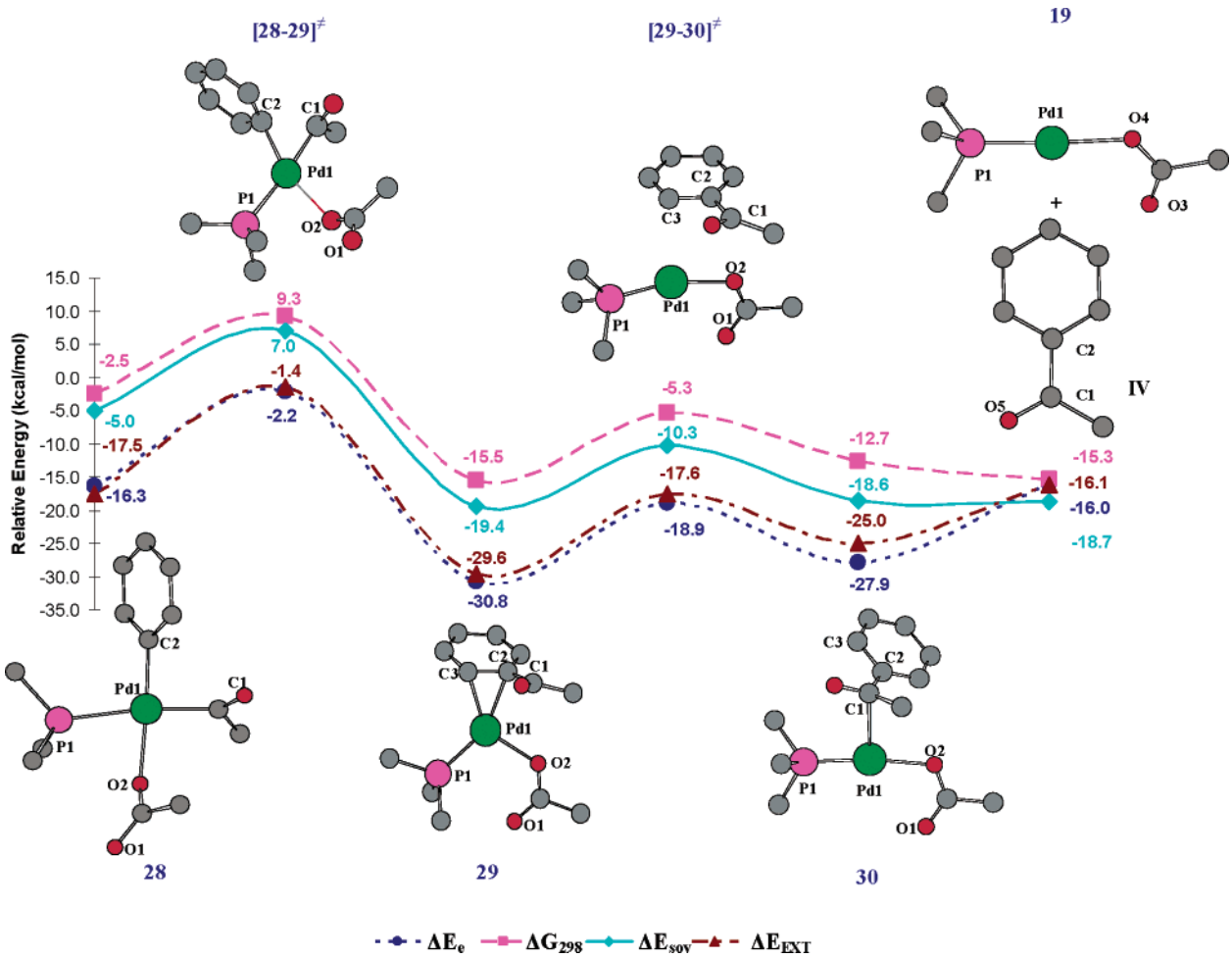

Figure 8. Energy profile for the reductive elimination process from **28** to **19**. For the conventions, see Figure 2.

point of the alternative transmetalation sequence (Figure 8). This reaction pathway also starts with the formation of a C−C bond between C(2) and C(1), which can be initiated by a gradual decrease of the C(2)−C(1) distance in **28**. In this first step, intermediate **29**, a π-complex of acetophenone, is formed in an exergonic reaction ($\Delta E_e = -14.5$ kcal/mol, $\Delta G_{298} = -13.0$ kcal/mol) which requires considerable activation ($\Delta E_e = 14.1$ kcal/mol, $\Delta G_{298} = 14.2$ kcal/mol). In the transition state **[28-29]**‡ the C(2)−C(1) distance is already as short as 1.911 Å and the C(2)−Pd−C(1) angle has decreased to 54.5°. The transition vector (327 *i*cm^{-1}) represents a narrowing of the C(2)−Pd−C(1) angle, with the acyl group and the aryl ring further approaching each other.

In the η^2-type π complex **29** (Figure 8), the C(2)−C(3) double bond of the phenyl ring is coordinated to the metal center (Pd(1)−C(2) = 2.203 Å and Pd(1)−C(3) = 2.199 Å). The NPA analysis indicates some electron transfer from the bonding π C(2)−C(3) orbital to an unoccupied orbital of the palladium along with back-donation from the d_π orbital of the metal to the π^* C(2)−C(3) orbital.

Further elongation of the Pd(1)−C(2) bond in **29** leads to the formation of intermediate **30**, in which the acetophenone remains loosely connected to the palladium via an interaction between its electrophilic carbonyl carbon and the electron-rich palladium center (Pd(1)−C(1) = 2.554 Å). Reaching the corresponding transition state **[29-30]**‡ requires less energy than the preceding step ($\Delta E_e = 11.9$ kcal/mol, $\Delta G_{298} = 10.3$ kcal/mol). In **[29-30]**‡ the Pd(1)−C(2) distance becomes much larger ((Pd(1)−C(2) = 3.248 Å in **[29-30]**‡ vs 2.203 Å in **29**) and the transition mode (39 *i*cm^{-1}) represents a motion of the phenyl fragment further away from the metal center. The resulting van der Waals complex **30** features a weak coordination of O(5), C(1), and C(2) to the metal center (Pd(1)−O(5) = 3.236 Å, Pd(1)−C(1) = 2.554 Å and Pd(1)−C(2) = 3.012 Å).

At this point, two pathways are conceivable for the complete decoordination of acetophenone (**IV**) from **30**. If no additional phosphine is present, dissociation of acetophenone directly leads to the two-coordinate complex **19** in an exergonic reaction ($\Delta E_e = 11.9$ kcal/mol, $\Delta G_{298} = -2.6$ kcal/mol). Acetophenone is also liberated when a phosphine (PMe_3) molecule approaches the intermediate **30**, which yields the three-coordinate palladium(0) species **1** in a substitution reaction ($\Delta E_e = 1.3$ kcal/mol, $\Delta G_{298} = -0.4$ kcal/mol) (Figure 9). Both of these pathways are computed to be very facile (see ΔG_{298} values), and therefore, the exact reaction conditions will determine which catalytic species is regenerated.

The structural parameters of all intermediates and transition states involved in the reductive elimination/ligand exchange sequence are summarized in Table 5. Selected NPA charges (Table S7) and more detailed structural data are available in the Supporting Information.

4. Discussion and Conclusions

In summary, mechanistically and energetically plausible catalytic cycles for the cross-coupling of phenylboronic acid with acetic anhydride have been identified, using either the three-coordinate anionic $[Pd(PMe_3)_2OAc]^-$ complex (**1**) or the two-coordinate anionic $[Pd(PMe_3)OAc]^-$ complex (**19**) as starting points. The oxidative addition of a molecule of acetic anhydride

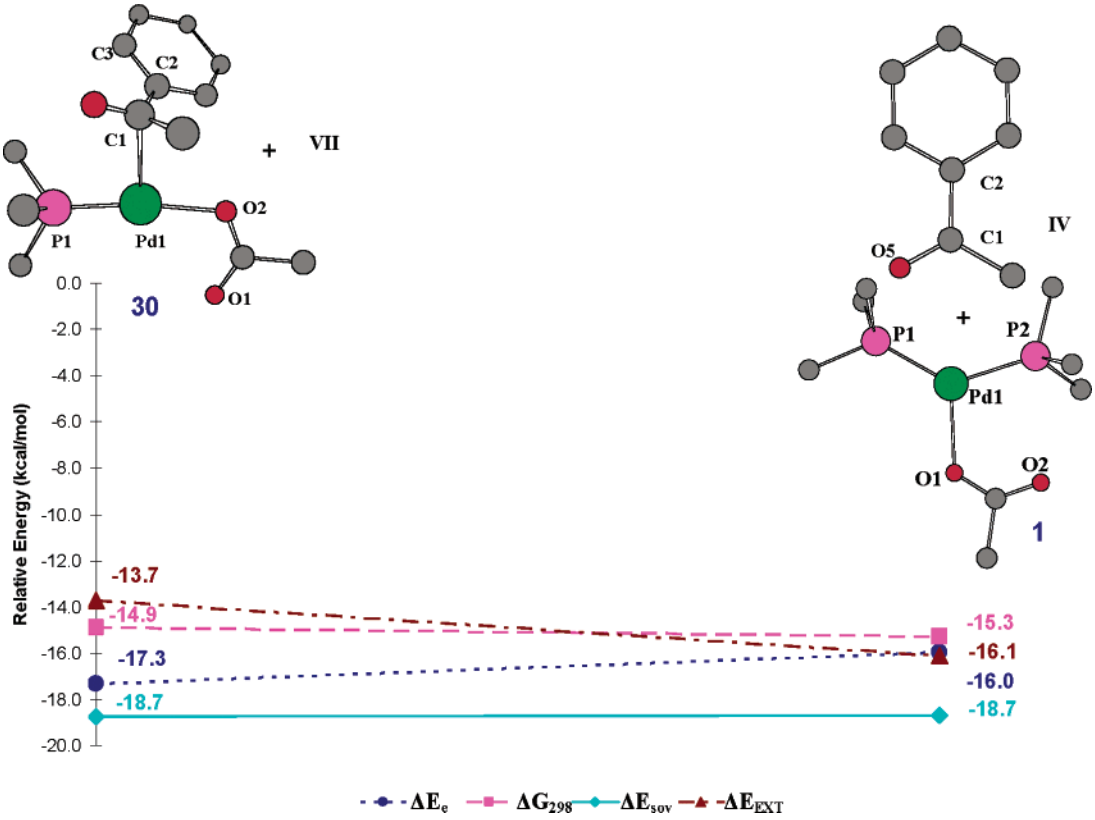

Figure 9. Pathway for the regeneration of tricoordinate catalyst **1**. For the conventions, see Figure 2.

Table 5. Optimized Geometric Parameters for Complexes [28-29]‡−30[a]

compd	Pd−P1	Pd−C1	Pd−C2	Pd−O1	Pd−O2	C2−C1	P−Pd−O2
[28-29]‡	2.398	2.112	2.059	4.048	2.275	1.911	79.7
29	2.299	2.798	2.203	3.517	2.666	1.493	106.0
[29-30]‡	2.183	3.571	3.248	3.226	2.182	1.497	165.8
30	2.215	2.554	3.012	3.086	2.174	1.521	172.5

[a] Bond distances are provided in angstroms and bond angles in degrees.

to either of the two species leads to the formation of anionic palladium(II) monophosphine complexes with two acetyl ligands located either cis (**5**) or trans (**23**) to each other. Starting from complex **23**, an alternative pathway for the transmetalation reaction with phenylboronic acid has been found that is dominated by trans-configured intermediates, in contrast to the previously described mechanism[6] starting from compound **5**. The product of this reaction sequence, intermediate **28**, is a suitable starting point for the reductive elimination of the product acetone. If a second phosphine molecule is provided, this step gives rise to the anionic bisphosphine complex **1**; otherwise, the monophosphine complex **19** is regenerated.

Figure 10 shows the energy profiles of all calculated reaction pathways for the catalytic cross-coupling of phenylboronic acid with acetic anhydride. The top part of the figure specifies the three phases of the catalytic cycle as well as the steps where the reactants are introduced (+**I**, +**II**) and where the products are liberated (−**III**, −**IV**). The data for the neutral cycle **12** → **5** → **9** → **12** (black) and the anionic cycle **1** → **5** → **9** → **1** (blue/black/blue) have been taken from our previous work,[6] where a correction of 10 kcal/mol per internal hydrogen bond has been applied for **6** and **8** to avoid differential stabilizing effects that will operate only in the gas phase and not in solution. Our present work provides data for the alternative anionic cycle **19** → **23** → **28** → **19** (green) and for the interconnections between different cycles (red) during oxidative addition (**1** → **23**, **19** → **5**) and reductive elimination (**9** → **19**, **28** → **1**).

Concerning the starting points of the three cycles in Figure 10, the reactants have been chosen to be **12** + **I** + **II** + $[PhB(OH)_2OAc]^-$ (**V**) for the neutral pathway, **1** + **I** + **II** for the previously studied anionic pathway, and **19** + **I** + **II** + PMe_3 (**VI**) for the new anionic pathway. The relative energy of the last two reactants is thus determined by the dissociation reaction **1** → **19** + PMe_3 (see Figure 1), which seems a natural choice. The relative energy of the starting point for the neutral cycle depends on the chosen source of acetate: we have argued previously[6] that it would seem realistic in view of the usual experimental conditions to provide acetate in the form of the Lewis adduct $[PhB(OH)_2OAc]^-$ (**V**), and we have adopted the same convention here. It should be stressed, however, that the relative position of the black curve in Figure 10 depends on this assumption: i.e., on the accessibility of acetate.

It is obvious from Figure 10 that the catalytic cycles even of this model reaction are quite complex and consist of many elementary steps. None of these steps requires excessive activation, since the individual barriers in Figure 10 are typically around 10 kcal/mol or even less. The largest barrier of 16.1 kcal/mol is found for the reaction **4** → **23**, which interconnects the two anionic pathways during oxidative addition. The other interconnections **20** → **5**, **11** → **19**, and **30** → **1** require energies of only 7.1, 11.9, and 1.3 kcal/mol, respectively. Judging from the energy profiles, all computed pathways appear to be feasible and should therefore be included in mechanistic considerations.

We now focus on a comparison of the two anionic pathways and refer to our previous work[6] for a discussion of the neutral pathway. The green profile in Figure 10 starting from the monophosphine anion $[Pd(PMe_3)OAc]^-$ (**19**) remains above the blue/black/blue profile starting from the diphosphine anion $[Pd(PMe_3)_2OAc]^-$ (**1**) throughout the cycle, the energy differ-

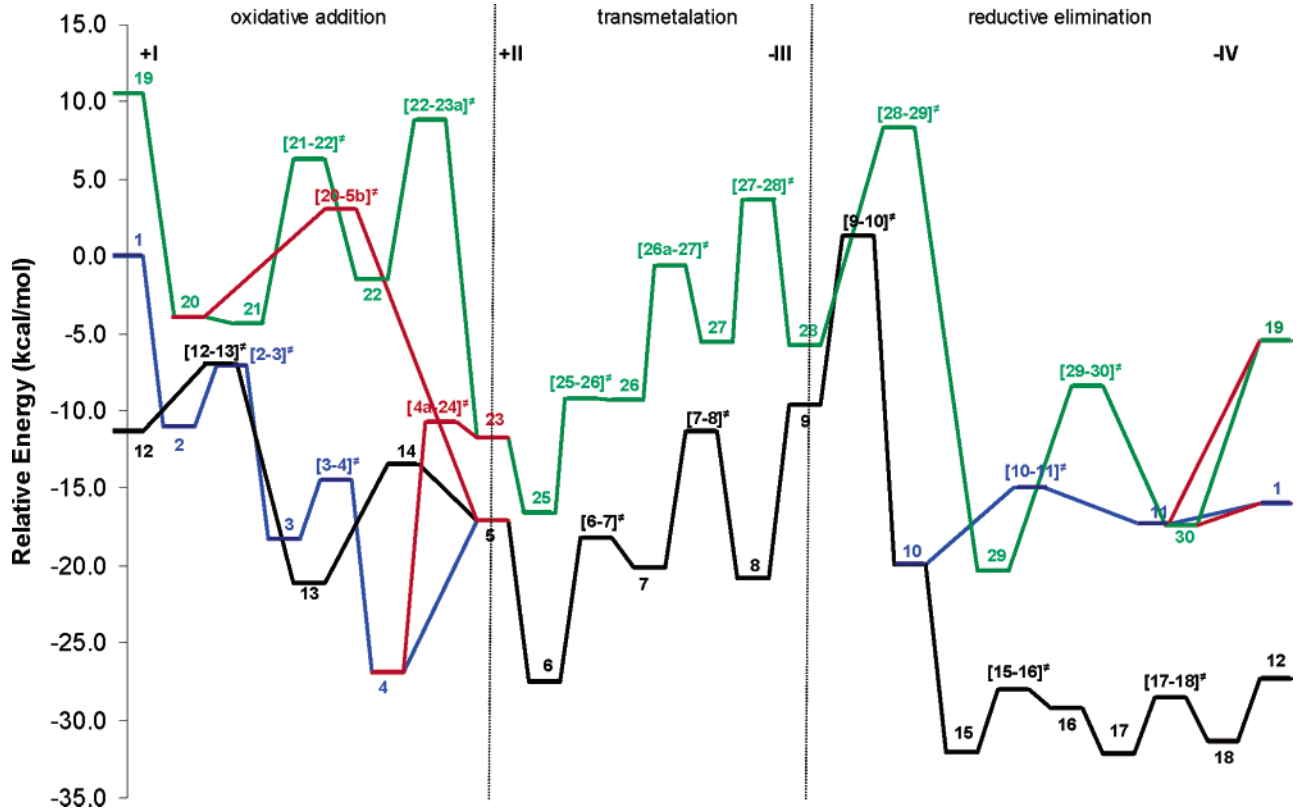

Figure 10. Relative energies (ΔE_e in kcal/mol) of the most significant intermediates and transition states involved in the catalytic cycles calculated in this work and in our previous work.[6]

ences being 10.6 kcal/mol at the beginning and end of the cycle (**19** vs **1**), 5.5 kcal/mol after oxidative addition (**23** vs **5**), and 4.2 kcal/mol after transmetalation (**28** vs **9**). On both anionic pathways, the oxidative addition is computed to be exothermic (by 17−22 kcal/mol), the transmetalation is slightly endothermic (by 6−8 kcal/mol), and the reductive elimination is slightly exothermic for **9** → **1** (by 6 kcal/mol) and essentially thermoneutral for **28** → **19**.

In both cases, the oxidative addition begins with the exothermic formation of an adduct (**2**, **21**) with acetic anhydride, which rearranges to a covalently bound complex (**3**, **22**) before undergoing the actual oxidative addition to a four-coordinate intermediate (**5**, **23**); the latter conversion is a two-step process in the case of **3** → **5** due to the need to split off one phosphine ligand, and a simple one-step process **22** → **23** in the case of the three-coordinate complex **22** (see Scheme 4). The transmetalation involves in both cases a crucial intermediate (**7**, **27**) with an η^2-bound phenyl ligand $PhB(OH)_2OAc$, while the other intermediates are different (hydrogen-bonded adducts **6** and **8**, Lewis adducts **25** and **26**); since both these paths have been confirmed by IRC calculations, it seems that the detailed course of transmetalation can be system dependent. Finally, in both cases, the reductive elimination starts with the formation of an η^2 π complex with the PhCOMe ligand (**10**, **29**), which requires some activation, whereas the subsequent steps are facile. The maximum individual energy barriers in Figure 10 for oxidative addition, transmetalation, and reductive elimination are 9.8, 11.2, and 11.0 kcal/mol in the diphosphine anionic cycle **1** → **5** → **9** → **1** and 10.6, 9.2, and 14.1 kcal/mol in the monophosphine anionic cycle **19** → **23** → **28** → **19**. These data, and inspection of Figure 10, indicate that these two anionic cycles are quite similar in many respects.

Figure 11 shows the free energy profiles for all pathways considered using the same conventions as in Figure 10. Both figures share a number of common features, but there are also notable differences. The relative positions of the starting points **1** and **12** are almost the same in both figures, while that of **19** is now much lower (−2.2 kcal/mol in Figure 11 vs 10.6 kcal/mol in Figure 10) due to the entropic contribution to the free energy of the reaction **1** → **19** + PMe_3 (see Figure 1). Generally speaking, dissociation reactions are entropically favored, while association reactions suffer from an entropic penalty because of the loss of translational and rotational degrees of freedom (typically around 10 kcal/mol at 298 K in the gas phase). The major differences between Figures 10 and 11 are caused by such entropic effects and occur in steps where reactants are added or products are liberated. One should keep in mind, of course, that these entropic effects will be less pronounced in solution due to solvation and desolvation, but they will still be present.

Closer inspection of Figure 11 confirms that the individual barriers remain moderate also on the free energy scale. The maximum such barriers for oxidative addition, transmetalation, and reductive elimination are 7.7, 11.2, and 12.3 kcal/mol in the diphosphine anionic cycle (**1** → **5** → **9** → **1**), 12.2, 10.3, and 11.8 kcal/mol in the monophosphine anionic cycle (**19** → **23** → **28** → **19**), and 19.7, 11.2, and 12.3 kcal/mol in the neutral cycle (**12** → **5** → **9** → **12**). The largest free energy barrier of 19.7 kcal/mol thus occurs during the oxidative addition on the neutral pathway. It is also obvious from Figure 11 that the interconnections between the pathways remain accessible in terms of free energy, since the most demanding such case, **4** → **23**, is associated with a free energy barrier of 15.0 kcal/mol.

Which of the catalytic cycles is the most favorable one? In a proper treatment of this problem, one would set up the kinetic equations for the intertwined catalytic cycles (Schemes 3 and 4) and solve them on the basis of the computed free energies (Figure 11). It is clear that this is extremely complex in the present case and that the results will depend on the actual

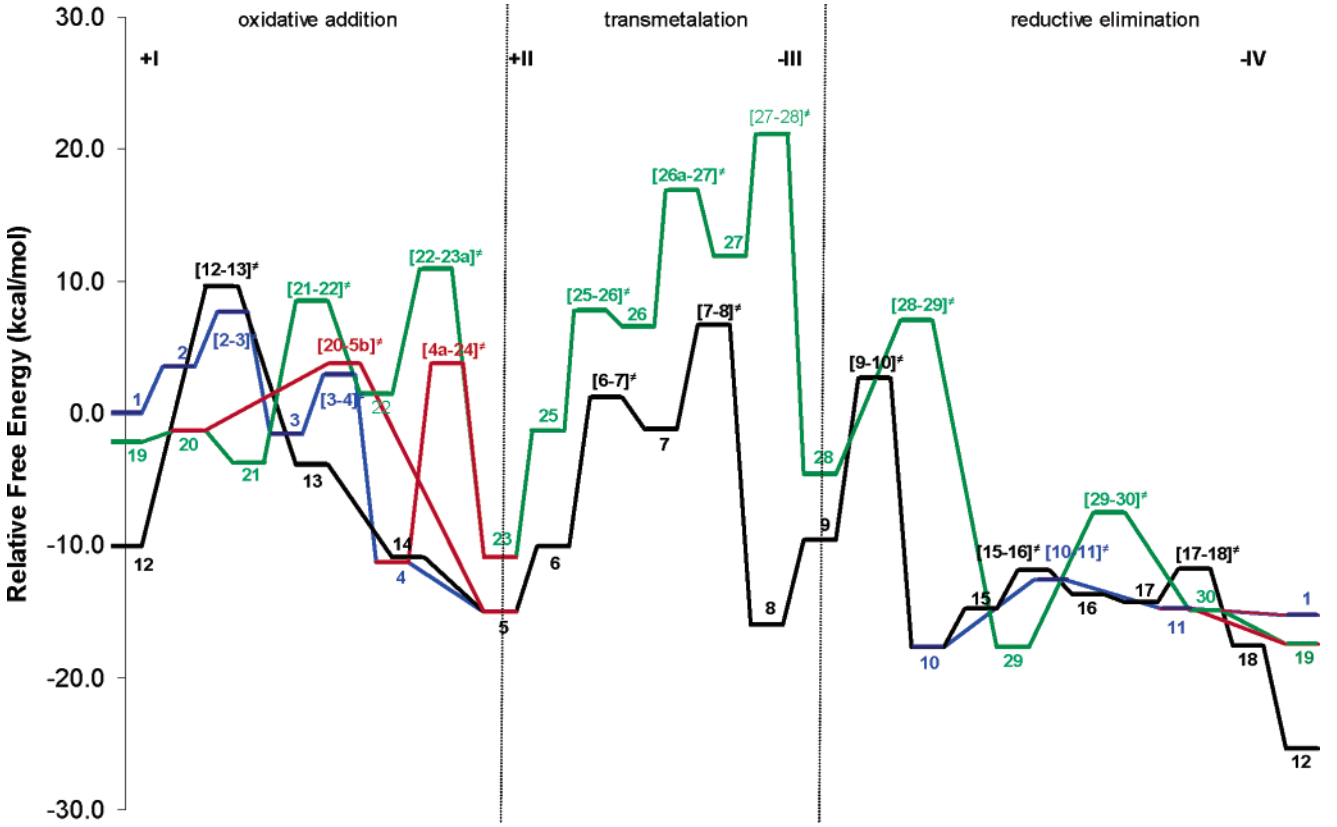

Figure 11. Relative free energies (ΔG_{298} in kcal/mol) of the most significant intermediates and transition states involved in the catalytic cycles calculated in this work and in our previous work.[6]

reaction conditions, and in particular on the concentrations; even in much simpler composite reactions, the results from such kinetic analysis can normally be interpreted in a useful manner only for certain limiting cases.[28] Given the need to resort to an approximate treatment, a common approach is to invoke a kinetic steady-state hypothesis and to assume that the concentration of the intermediates remains constant in an efficient catalytic cycle.[28] One can then deduce that the maximum rate of the cycle is proportional to $\exp(-\Delta G_{max}/RT)$, where ΔG_{max} is the free energy span of the cycle: i.e., the free energy difference between the highest and lowest point.[29] The largest possible rate (highest turnover number) of the catalytic cycle is obtained for the lowest free energy span.[29]

Following recent precedent[14] we apply this concept to the cycles in Figure 11. In addition to the three cycles discussed up to now, two further anionic cycles are present in Figure 11 when considering interconnections, namely **1** → **23** → **28** → **1** and **19** → **5** → **9** → **19**. Table 6 lists the free energy spans for all five cycles, as well as the overall and the largest individual free energy barriers. In terms of the free energy span, the diphosphine anionic cycle (**1** → **5** → **9** → **1**) and the interconnected monophosphine anionic cycle (**19** → **5** → **9** → **19**) are the most favorable, with a slight edge for the latter. These two cycles are also associated with the lowest overall and individual free energy barriers (Table 6). The alternative anionic cycles proceed via less stable intermediates and, hence, a less advantageous transmetalation route (**23** → **28** rather than **5** → **9**, see Figure 11), and they are therefore not competitive. The neutral cycle suffers from the large free energy barrier for oxidative addition.

Table 6. Free Energy Data (kcal/mol) for Catalytic Cycles in Figure 11

cycle	type[a]	ΔG_{max}[b]	$\Delta G_{max}^{\ddagger}$[c]	$\Delta G_{i,max}^{\ddagger}$[d]
1 → **5** → **9** → **1**	a2	27.6	7.7	12.3
19 → **23** → **28** → **19**	a1	38.9	23.4	12.2
12 → **5** → **9** → **12**	n2	35.7	19.7	19.7
1 → **23** → **28** → **1**	a2	38.9	21.2	12.2
19 → **5** → **9** → **19**	a1	24.4	8.9	12.3

[a] Legend: a2, anionic diphosphine; a1, anionic monophosphine; n2, neutral diphosphine. [b] Free energy span, difference between the highest and lowest points of the catalytic cycle. [c] Overall free energy barrier, difference between the highest point and the starting point. [d] Largest free energy barrier for any individual step.

In summary, our calculations favor the two anionic cycles specified above. Experimentally, the fastest turnover is observed for this coupling reaction if anionic palladium species are present, and just enough phosphine is added to keep the palladium in solution while excess phosphine retards the reaction.[4,12,13] These experimental findings are consistent with an interconnected monophosphine anionic cycle (**19** → **5** → **9** → **19**).

Given the limitations of our computational approach which have been discussed in this paper and in our preceding paper,[6] one should emphasize the qualitative conclusions that emerge from our calculations. While we have attempted to identify the "best" catalytic cycle for the reaction studied presently, we have actually found several catalytic pathways that are interconnected and may contribute to catalytic turnover. In the present case, anionic pathways seem to be preferred, but the balance between the competing pathways can clearly be affected by the reaction conditions. Likewise, when one goes from the current simplified model system to other Suzuki-type palladium-catalyzed cross-coupling reactions, this balance can shift again. In view of this mechanistic complexity, further studies are needed to better

(28) Laidler, K. J. *Chemical Kinetics*, 3rd ed.; Harper and Row: New York, 1987.
(29) Amatore, C.; Jutand, A. *J. Organomet. Chem.* **1999**, *576*, 254.

understand the course of Suzuki-type reactions with catalysts that are commonly used in real-life experiments (e.g., triarylphosphine−palladium complexes).

Acknowledgment. We thank Prof. Dr. A. Jutand for helpful suggestions and discussions. We are grateful to the DFG and the BMBF for financial support. L.J.G. thanks Prof. Dr. M. T. Reetz for his constant encouragement and generous support. D.K. thanks Prof. Dr. V. R. Jensen, Dr. M. Bühl, Dr. H. M. Senn, Dr. S. Vyboishchikov, and H. U. Wüstefeld for fruitful and stimulating discussion.

Supporting Information Available: Tables, text, and figures giving energies, graphical representations, geometrical parameters, NPA charges, Cartesian coordinates of all DFT optimized structures, and complete ref 18. This material is available free of charge via the Internet at http://pubs.acs.org.

OM050685H